European Cells and Materials Vol.55 2026 (pages 17–31) DOI: 10.22203/eCM.v055a02 ISSN 1473-2262

Original Article

PHOTO-CROSSLINKED HYDROGEL FOR ENHANCED BONE DEFECT REGENERATION VIA SUSTAINED RELEASE OGP(10-14)

L.Y. Liu[1,§], F.C. Zeng[1,2,§], Y.W. He[1], S.W. Dong[1,3,*] and J.M. Li[1,*]

[1]Department of Biomedical Materials Science, School of Biomedical Engineering, Third Military Medical University, 400038 Chongqing, China
[2]Guangdong Key Laboratory for Biomedical Measurements and Ultrasound Imaging, National-Regional Key Technology Engineering Laboratory for Medical Ultrasound, School of Biomedical Engineering, Medical School, Shenzhen University, 518060 Shenzhen, Guangdong, China
[3]State Key Laboratory of Trauma and Chemical Poisoning, Third Military Medical University, 400038 Chongqing, China
[§]These authors contributed equally.

Abstract

Background: Currently, the clinical treatment of severe bone defects remains a major challenge. Gelatin methacryloyl (GelMA) hydrogels with extracellular matrix (ECM)-like properties are commonly used materials for bone defect repair. However, due to the lack of osteogenic activity, researchers have considered using tissue engineering methods to address this issue. **Methods:** A composite hydrogel scaffold was fabricated by incorporating acryloylated polyethylene glycol N-hydroxysuccinimide (AC-PEG-NHS)-modified osteogenic growth peptide (OGP)(10-14) (AC-PEG-OGP(10-14)) and primary osteoblasts into a GelMA matrix. The hydrogel scaffold was characterized using scanning electron microscopy (SEM), mechanical testing, and the bicinchoninic acid (BCA) protein assay. *In vitro*, the effects of the scaffold on the differentiation of osteoblasts and bone marrow-derived macrophages (BMMs) were evaluated. *In vivo*, its role in bone defect repair was assessed using a rat model. **Results:** The results demonstrated that the AC-PEG-OGP(10-14)-loaded hydrogel scaffold significantly enhanced the mechanical properties and slowed the degradation rate based on the GelMA scaffold, and it could also achieve the controlled release of the osteogenic peptide OGP(10-14). *In vitro* and *in vivo* experiments showed that the material exhibited excellent biocompatibility and osteogenic mineralization properties. It inhibited osteoclast formation, thereby significantly promoting the repair of mouse femoral bone defects. The underlying mechanism is closely related to the activation of the Wnt/*β-catenin* signaling pathway. **Conclusions:** AC-PEG-OGP(10-14)-loaded hydrogel scaffold offers an effective solution for repairing bone defects and significantly enhances bone regeneration.

Keywords: GelMA, OGP(10-14), bone defect repair, tissue engineering.

***Address for correspondence**: S.W. Dong, Department of Biomedical Materials Science, School of Biomedical Engineering, Third Military Medical University, 400038 Chongqing, China. Email: dongshiwu@tmmu.edu.cn; J.M. Li, Department of Biomedical Materials Science, School of Biomedical Engineering, Third Military Medical University, 400038 Chongqing, China. Email: lijianmei@tmmu.edu.cn.

Introduction

Bone defects of critical size caused by trauma, tumors, and osteoporosis are common conditions in the field of orthopedics [1,2]. Such conditions may lead to localized dysfunction, which in turn affects the patient's daily life and mobility, posing a serious threat to the patient's physical and mental health. Bone grafting has been widely used as a conventional treatment for bone defects in orthopedics. Commonly used materials for bone defect repair include autogenous bone, allograft bone, xenograft bone, polymer materials, and periosteum-induced materials [3,4]. However, due to problems of origin, potential ethical issues, immune rejection, and insufficient osteogenic capacity, a completely ideal bone repair material does not exist [5,6]. At present, study has shown that bone tissue engineering can simulate the process of tissue repair by carrying cells and growth factors in scaffold materials, which has important application prospects in the treatment of large bone defects [7].

Bone tissue regeneration is a complex and intricate process that involves the interaction of multiple growth factors, such as bone morphogenetic protein (BMP)-2, BMP-9, concentrated growth factors (CGF), and other growth factors [8–10]. These factors directly affect the prolifer-

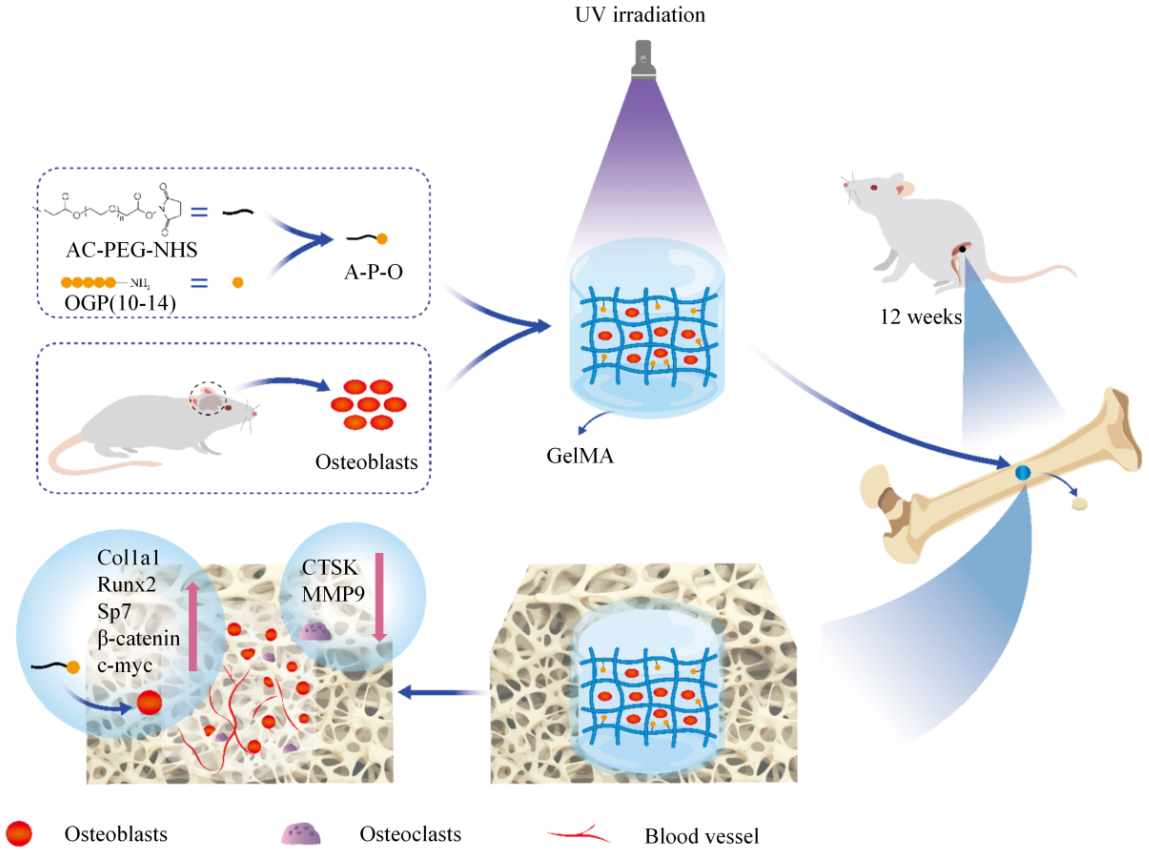

Fig. 1. Schematic illustration of the fabrication of OGP(10-14)-loaded sustained-release hydrogels and their application in promoting bone regeneration. The figures were partially designed with Adobe Illustrator (version Illustrator 28.x, USA). A-P-O = AC-PEG-OGP(10-14).

ation, migration, and differentiation of bone-related cells. Currently, studies have reported that the combination of growth factors and scaffold materials can promote bone defect repair [11–13]. Among these growth factors, osteogenic growth peptide (OGP) is a highly conserved natural polypeptide present in the human body. It is composed of 14 amino acids and is resistant to high temperatures and organic solvents [14,15]. During hydrolysis, OGP produces a C-terminal pentapeptide (Tyr-Gly-Phe-Gly-Gly), known as OGP(10-14). Studies have demonstrated that OGP(10-14) promotes the proliferation, differentiation, and mineralization of osteoblasts [16,17] and regulates the expression of transforming growth factors, insulin-like growth factors, and basic fibroblast growth factors, all of which increase *in vivo* bone formation and bone mineral density (BMD) of trabecular bone [18,19]. OGP(10-14) is the smallest fragment of OGP with biological activity, and its structure is relatively stable; thus, OGP is suitable for the clinical treatment of bone defect repair as an additional bone growth factor. However, how to effectively control the release of OGP(10-14) remains one of the key issues to be solved in the field of bone defect repair. As a chemical cross-linking molecule, acryloylated polyethylene glycol N-hydroxysuccinimide (AC-PEG-NHS) has an NHS group at one end that can bind to the amino groups of amino acids, forming stable amide bonds, and an AC group at the other end that can react with materials capable of photopolymerization [20,21]. Therefore, compared with the simple method of mixing OGP(10-14) with material physics, AC-PEG-NHS, as the connecting molecule, can specifically bind to OGP(10-14), significantly prolonging the release time of this peptide and effectively avoiding the burst release phenomenon, thereby achieving a more controllable sustained-release effect.

Gelatin methacryloyl (GelMA) retains the core functional sequences of the extracellular matrix (ECM). It also possesses unique photo-crosslinking properties, enabling it to solidify into a hydrogel under specific light irradiation [22]. These characteristics endow GelMA with injectability, rapid gelation, suitability for customized bioprinting,

and ease of cell seeding; thus, it is widely used in the field of bone defect research [23,24]. In addition, studies have found that GelMA can enhance cellular mechanical transduction and promote osteogenic differentiation of stem cells [25,26], and the use of cell-loaded GelMA can enhance bone defect repair [27–30].

In this study, the researchers cross-linked AC-PEG-NHS with OGP(10-14) and loaded the resulting complex onto a GelMA scaffold together with primary osteoblasts, thereby synthesizing a novel controlled-release hydrogel (Fig. 1). This research further analyzed the relevant physicochemical properties of this material *in vitro* and *in vivo*, evaluated its biocompatibility, and elucidated the effects of the novel sustained-release hydrogel on the repair of mouse femoral bone defects, with the goal of providing a new strategy for bone defect repair.

Materials and Methods

Materials

The following materials were used in this study: gelatin methacryloyl (EFL-GM-90, EFL, Suzhou, China), OGP(10-14) (HY-107024, MCE, Monmouth Junction, NJ, USA), AC-PEG-NHS (EFL-AC-PEG-NHS-2K, EFL, Suzhou, China), Ham's F-12 nutrient mixture (F-12) (11765054, Gibco, Grand Island, NY, USA), fetal bovine serum (C0234, Gibco, Grand Island, NY, USA), Calcein-AM/PI cell activity and cytotoxicity assay kit (C2015M, Beyotime, Shanghai, China), WST-1 cell proliferation and cytotoxicity assay kit (C0035, Beyotime, Shanghai, China), osteogenic induction medium (MUXMX-90021, OriCell, Suzhou, China), recombinant mouse macrophage colony-stimulating factor (M-CSF) (CB34, Novoprotein, Suzhou, China), recombinant mouse receptor activator of nuclear factor-κB ligand (RANKL) (C28A, Novoprotein, Suzhou, China), α-Minimum Eagle's Medium (α-MEM) (C12571500BT, Gibco, USA), twelve-week-old C57BL/6 mice (C57BL/6, Charles River, Wilmington, MA, USA), bicinchoninic acid (BCA) protein assay kit (BL521A, Biosharp, Hefei, China), mouse granulocyte-macrophage colony-stimulating factor (GM-CSF) ELISA kit (EK0365, Boster, Wuhan, China), and mouse interferon-γ (IFN-γ) ELISA kit (EK0375, Boster, China).

Fourier Transform Infrared Spectroscopy (FTIR)

A sample of AC-PEG-NHS (0.8 mg) was mixed with 200 μL of an OGP(10-14) solution (the concentration of OGP(10-14) was 10 mM). The mixture was incubated in the dark at 4 °C for 20 hours. After incubation, the solution was lyophilized to obtain a powder. An FTIR spectrometer (Spectrum Two, PerkinElmer, Waltham, MA, USA) was used to analyze the lyophilized powder and pristine AC-PEG-NHS powder. After scanning was completed, the data were saved in Excel format. Data processing software was subsequently used to analyze the obtained data.

Scanning Electron Microscopy (SEM)

Lithium phenyl-2,4,6-trimethylbenzoylphosphinate (LAP) was added to GelMA as a photoinitiator at a concentration of 0.25 % (w/v). The mixture was protected from light and heated in a water bath at 63 °C until completely dissolved, with periodic agitation during the process to obtain the GelMA solution. The incubated AC-PEG-OGP(10-14) was mixed with GelMA solution and then irradiated with UV light (405 nm, 3 W) at a distance of 10 cm for 30 seconds to generate the AC-PEG-OGP(10-14) group composite material (the concentration of AC-PEG-OGP(10-14) was 10^{-7} mM). Following the same procedure, OGP(10-14) was mixed with GelMA solution to constitute OGP(10-14) group composite material (the concentration of OGP(10-14) was 10^{-7} mM), and GelMA group material without OGP(10-14) peptide. The microstructure of the materials was observed using SEM (ZEISS Cross Beam 340, Carl Zeiss AG, Oberkochen, Germany), and the pore size was calculated using ImageJ software (1.53k, NIH, Bethesda, MD, USA).

C57BL/6 neonatal mice were purchased from the Third Military Medical University. Neonatal mice were euthanized by an overdose of sodium pentobarbital injection, and primary osteoblasts were isolated from their calvariae. The osteoblasts were subsequently cultured in complete F-12 medium. After the osteoblasts were passaged to the third generation, they were implanted into three groups of materials and prepared into three groups of biomaterials: the GelMA group, OGP(10-14) group and AC-PEG-OGP(10-14) group. Each biomaterial was adjusted to a cell density of 1×10^6 cells/mL. The growth of osteoblasts within the biomaterials was observed using SEM.

Pore Measurement Experiment

The porosity was evaluated using the liquid displacement method [31,32]. The dimensions of the samples were recorded, and their volume (V) was calculated. The initial weight (W_0) of each sample was measured before immersion in anhydrous ethanol for 24 hours. After immersion, the weight (W_p) was recorded, and the porosity was calculated using the following equation:

$$\text{Porosity } \% = \frac{(W_p - W_0)}{\rho V} \times 100\ \% \quad (1)$$

Where ρ is the density of anhydrous ethanol (0.79 g/cm^3).

Assessment of Mechanical Properties

Considering the three groups of materials, 200 μL of GelMA, OGP(10-14), and AC-PEG-OGP(10-14) were respectively added to the molds. The hydrogel was subsequently induced by irradiation with a 405 nm near-ultraviolet flashlight for 30 seconds. The resulting cylindri-

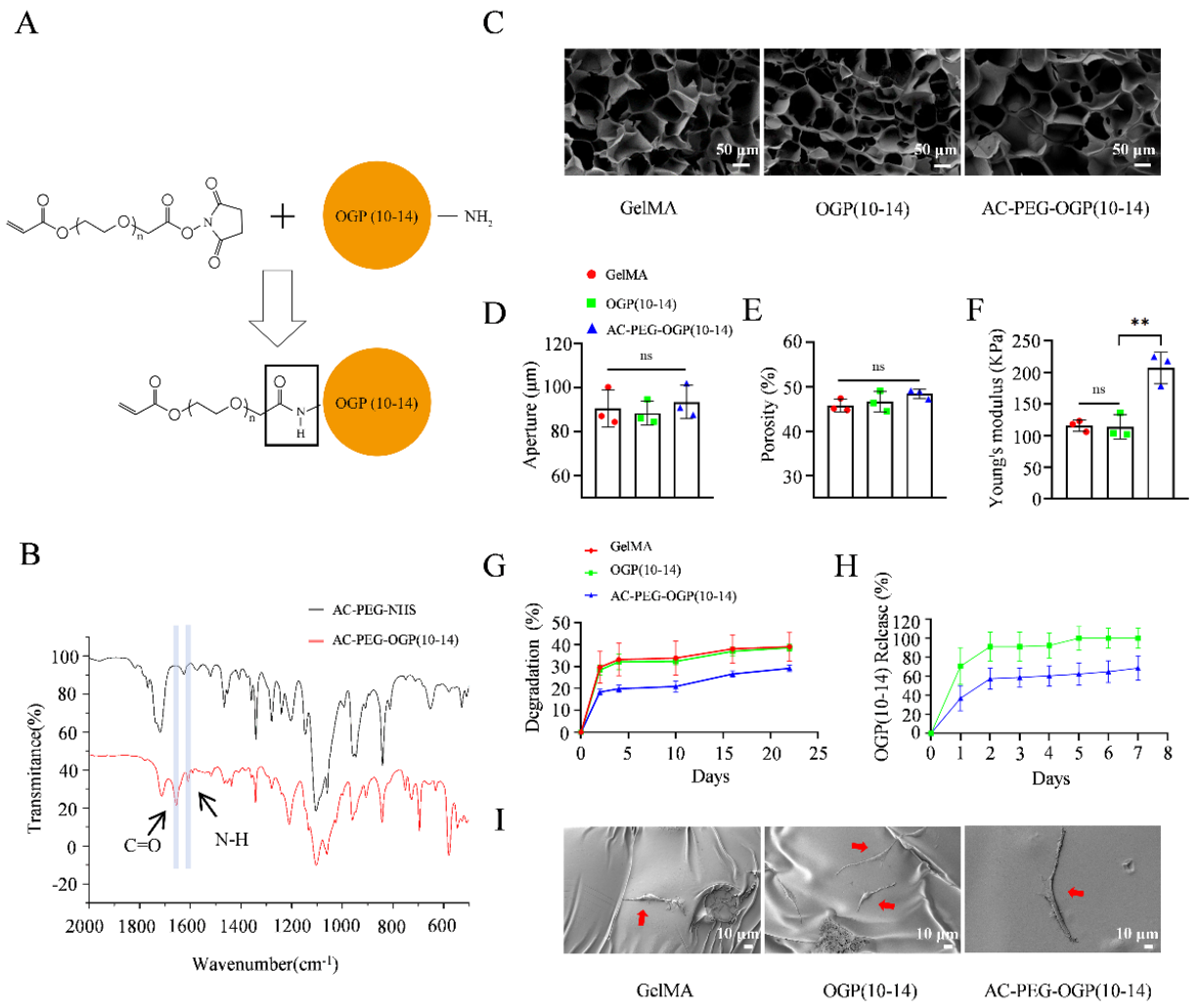

Fig. 2. Characterization of the materials. (**A**) Schematic representation of the reaction between AC-PEG-NHS and OGP(10-14) to form AC-PEG-OGP(10-14). The figure was designed with Adobe Illustrator (version Illustrator 28.x, USA). (**B**) FTIR spectra of AC-PEG-NHS and AC-PEG-OGP(10-14). (**C**) Cross-sectional SEM view of the composite materials. The scale bar represents 50 μm. (**D**) Pore size distribution of the materials. (**E**) Porosity assessment of the materials. (**F**) Young's modulus measurements of the materials. (**G**) Cumulative degradation of the materials. (**H**) Cumulative release of composite OGP(10-14). (**I**) SEM images of biological materials loaded with osteoblasts. The red arrows point to osteoblasts. n = 3. ns, not significant; $^{**}p < 0.01$. The scale bar represents 10 μm.

cal hydrogels were vertically positioned at the center of the lower compression plate of the mechanical testing instrument (TA ElectroForce LMI 400N, TA Instruments, New Castle, DE, USA), ensuring that no tilt occurred. Compression testing was then performed at a rate of 0.01 mm/s until sample fracture. The stress-strain curves of the different material groups were recorded and saved.

Materials Degradation Experiment

Three groups of materials, GelMA, OGP(10-14) and AC-PEG-OGP(10-14), were subjected to freeze-drying treatment, and their initial masses (W_0) were recorded. The materials were subsequently immersed in phosphate buffered saline (PBS) and placed in a constant temperature incubator at 37 °C. After 2 days, the supernatant was removed, followed by another freeze-drying process to record the mass at this stage (W). The materials were then re-immersed in PBS. This procedure was repeated at specified time points on Days 4, 10, 16, and 22. The degradation rate was calculated by using formula (2):

$$\text{Degradation } \% = \frac{W_0 - W}{W_0} \times 100\ \% \qquad (2)$$

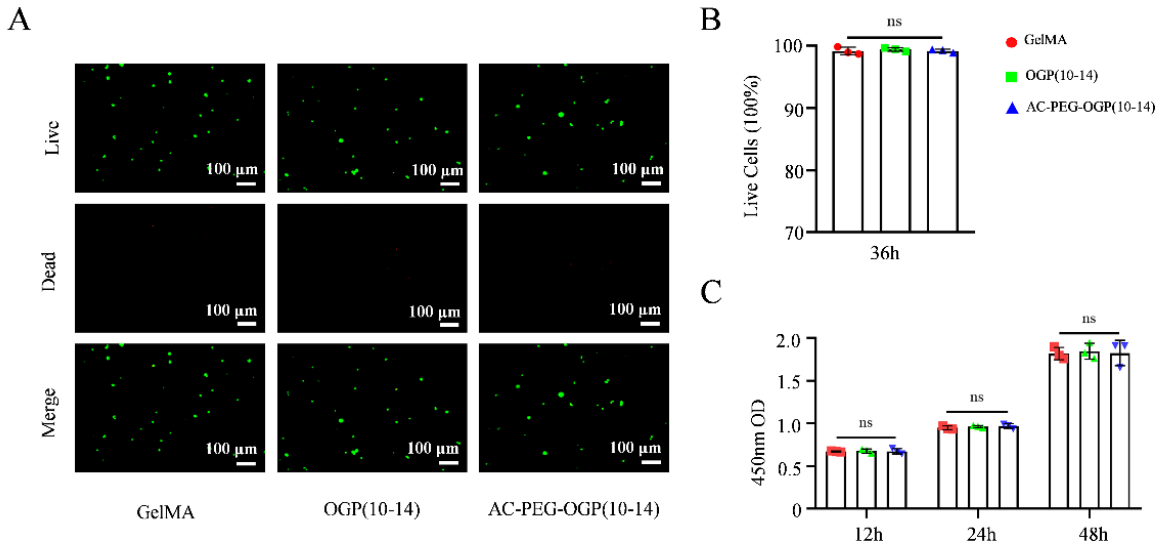

Fig. 3. *In vitro* evaluation of the biocompatibility of hydrogels in different groups. (**A**) Calcein-AM/PI staining image. (**B**) Survival rate of osteoblasts. (**C**) Proliferation of primary osteoblasts. n = 3. ns, not significant. The scale bar represents 100 μm.

Where W is the weight after each degradation.

In Vitro Release Experiments of OGP(10-14) Peptide

The three groups of prepared materials, GelMA, OGP(10-14) and AC-PEG-OGP(10-14), were immersed in PBS and placed in a constant temperature incubator at 37 °C. The material extract was collected daily, and fresh PBS was added. This process was repeated for a total of 7 days of collection. The collected material extract was analyzed using a BCA protein assay kit to measure the optical density (OD), and the cumulative release of OGP(10-14) was calculated.

Cell Compatibility Experiment

Osteoblasts were implanted into three groups of materials to generate the three groups of biomaterials, GelMA, OGP(10-14) and AC-PEG-OGP(10-14), and the proliferation of cells in the biomaterials was analyzed using a WST-1 cell proliferation and cytotoxicity assay kit. WST-1 solution was added to 96-well plates, and the OD values were measured at 12 hours, 24 hours, and 48 hours. Cell cytotoxicity was assessed using a Calcein-AM/PI Cell Activity and cytotoxicity assay kit, and fluorescence microscopy imaging (ZOE^{TM} Fluorescent Cell Imager, 1450031, Bio-Rad, Hercules, CA, USA) was used to determine live/dead cells on the biomaterials.

In Vitro Osteoblast Differentiation Experiments

Osteogenic Differentiation with Biomaterials

After the three groups of biomaterials, GelMA, OGP(10-14) and AC-PEG-OGP(10-14), were cultured in osteogenic medium for 7 days, the messenger RNA (mRNA) expression of the osteogenic differentiation genes *Runx2*, *Sp7*, *Col1a1*, *β-catenin*, and *c-myc* was examined using reverse transcription quantitative polymerase chain reaction (RT-qPCR). Primer sequences are provided in **Supplementary Table 1**. Staining was performed using an alkaline phosphatase (ALP) staining kit. After 14 days of culture, the biomaterials GelMA, OGP(10-14), and AC-PEG-OGP(10-14) were stained with Alizarin Red S (ARS) staining solution.

Co-Culture Osteogenic Differentiation Experiments

The GelMA, OGP(10-14), and AC-PEG-OGP(10-14) biomaterials were cultured in F-12 medium. Extracts were collected daily over both 7-day and 14-day periods. These extracts were used to prepare osteoblast co-culture media. Following 7 days of co-culture with osteoblasts in culture plates, osteogenic differentiation-related gene mRNA expression levels were analyzed using RT-qPCR, and the cells were stained with ALP reagent. After 14 days of co-culture under identical conditions, the cells were stained with ARS solution. Stained samples were examined under microscopy (Motic SMZ-171, Motic China Group, Xiamen, China), and representative images were captured. The images were analyzed using ImageJ software to calculate

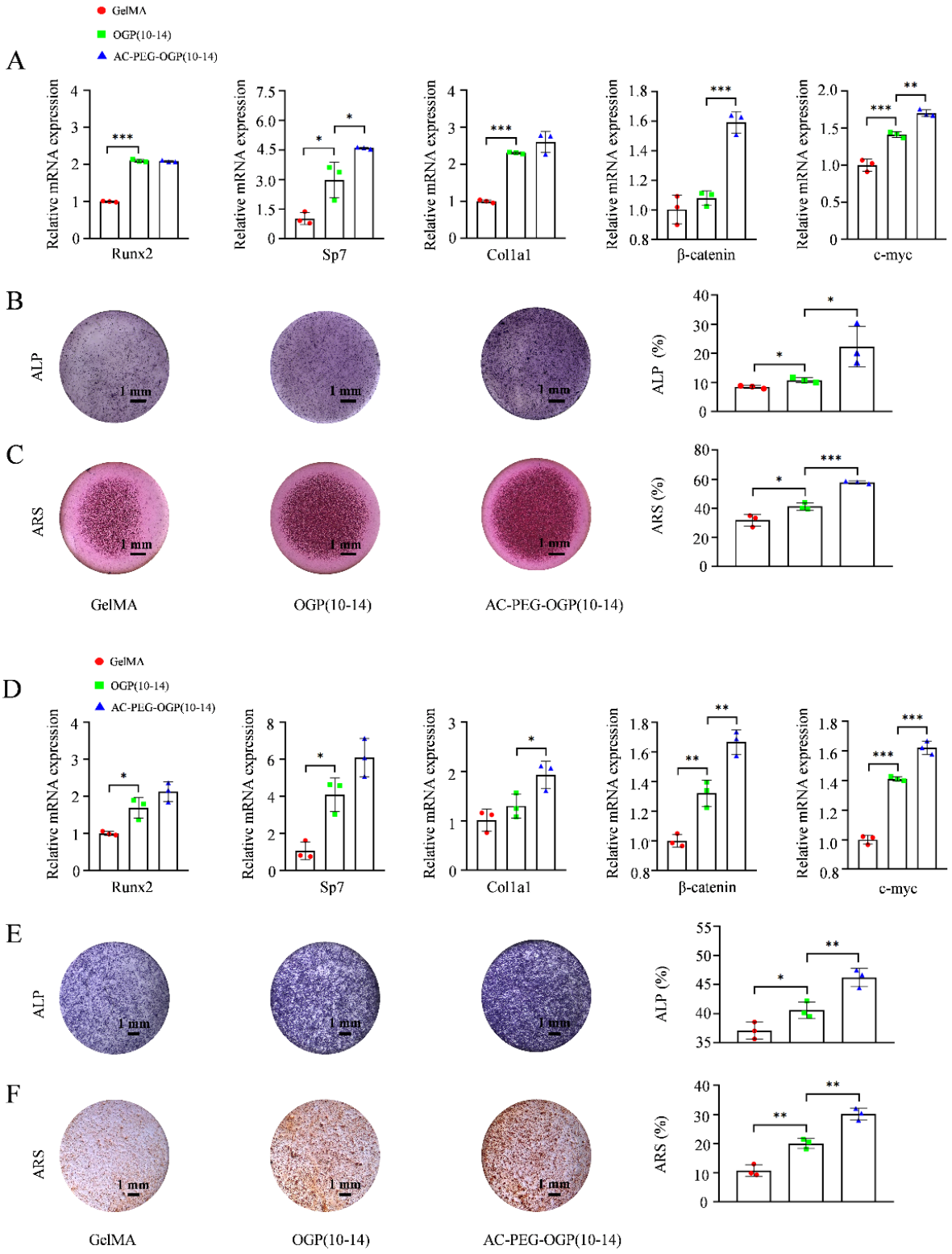

Fig. 4. Sustained-release hydrogels promote osteoblast differentiation *in vitro*. (**A**) mRNA expression of osteogenesis-related genes in primary osteoblasts. (**B**) ALP staining results and quantification of the staining area. (**C**) ARS staining results and quantification of the staining area. (**D**) mRNA expression of osteogenesis-related genes in co-cultured primary osteoblasts. (**E**) ALP staining results and quantification of the staining area of co-cultured primary osteoblasts. (**F**) ARS staining results and quantification of the staining area of co-cultured primary osteoblasts. n = 3. *$p < 0.05$; **$p < 0.01$; ***$p < 0.001$. The scale bar represents 1 mm.

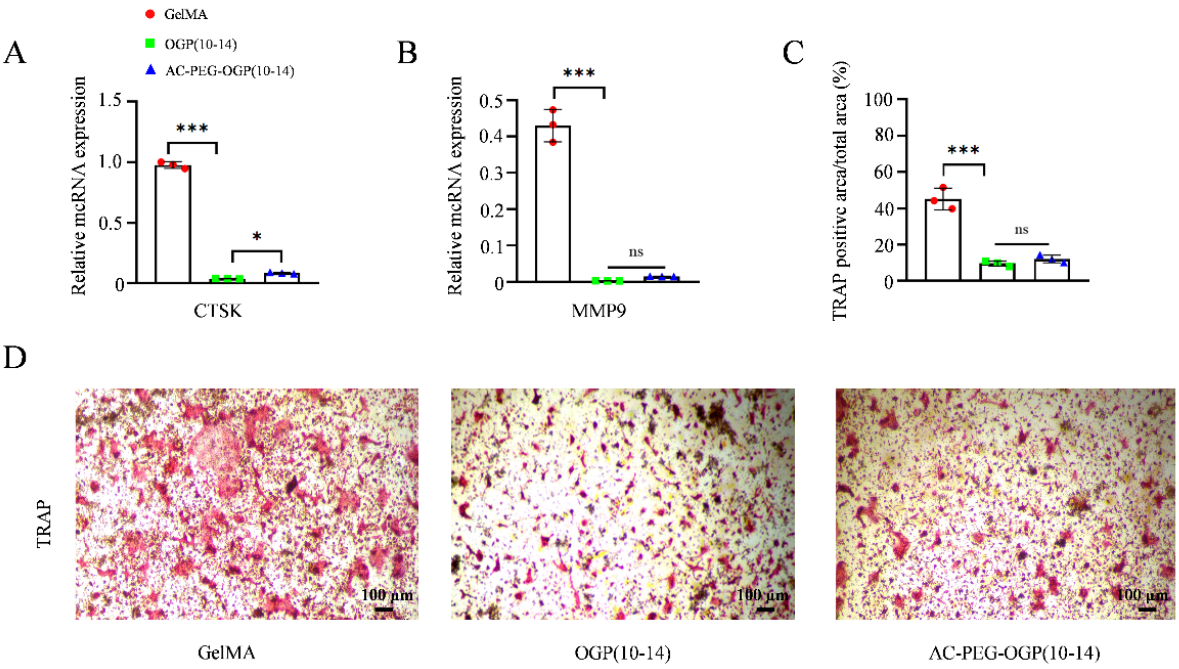

Fig. 5. Effects of different hydrogels on osteoclast differentiation in BMMs *in vitro*. (**A**) mRNA expression levels of *CTSK*. (**B**) mRNA expression levels of *MMP9*. (**C**) Quantification of the TRAP staining area. (**D**) TRAP staining images. n = 3. ns, not significant; *$p < 0.05$; ***$p < 0.001$. The scale bar represents 100 μm.

the percentage of the area that was positively stained in the entire field of view.

In Vitro Bone Marrow-Derived Macrophage (BMM) Differentiation Co-Culture Experiment

Five-week-old C57BL/6 mice were purchased from the Third Military Medical University. Five-week-old C57BL/6 mice were euthanized by an overdose of sodium pentobarbital injection, and BMMs were isolated from their femurs and tibias. The extracts of three groups of biomaterials, namely, GelMA, OGP(10-14), and AC-PEG-OGP(10-14), were collected daily for four consecutive days. The extracts were then used to prepare co-culture media containing RANKL (100 ng/mL) and M-CSF (50 ng/mL). This medium was used to co-culture BMMs in culture plates for 4 days. The mRNA expression levels of *CTSK* and *MMP9* were subsequently detected using RT-qPCR. Primer sequences are provided in **Supplementary Table 1**. Additionally, staining was performed using a tartrate-resistant acid phosphatase (TRAP) staining kit, and the stained cells were observed and imaged under a microscope (DMIL LED, Leica, Wetzlar, Germany) for further analysis.

Construction of Animal Models

Twelve-week-old C57BL/6 mice were purchased from Charles River Laboratories and maintained at the Third Military Medical University. The mice were acclimatized for approximately one week under controlled temperature and humidity conditions prior to experimentation. The mice were randomly divided into four groups, with three mice in each group. Three groups of biomaterials, namely, GelMA, OGP(10-14), and AC-PEG-OGP(10-14), were prepared in advance and cultured in complete F-12 medium. The biomaterials to be implanted were cut to appropriate sizes before the procedure. The mice were anesthetized with sodium pentobarbital. Hair was removed from the femoral region, and the area was disinfected with iodine tincture. The skin and subcutaneous tissues were separated to expose the midshaft of the femur, and a 1.6-mm diameter hole was drilled along the central axis of the femur. The mice were divided into four groups according to the type of implant material: the control group (no material implanted), GelMA group (GelMA material implanted), OGP(10-14) group (OGP(10-14) material implanted), and AC-PEG-OGP(10-14) group (AC-PEG-OGP(10-14) material implanted). After implantation, the muscles and skin were sutured using absorbable sutures. The mice were allowed free movement and unrestricted access to food and water postoperatively. After 4 weeks of breeding, the mice were anesthetized with sodium pentobarbital. Blood was collected from the retro-orbital plexus, and serum was obtained. An overdose of anesthetic was subsequently ad-

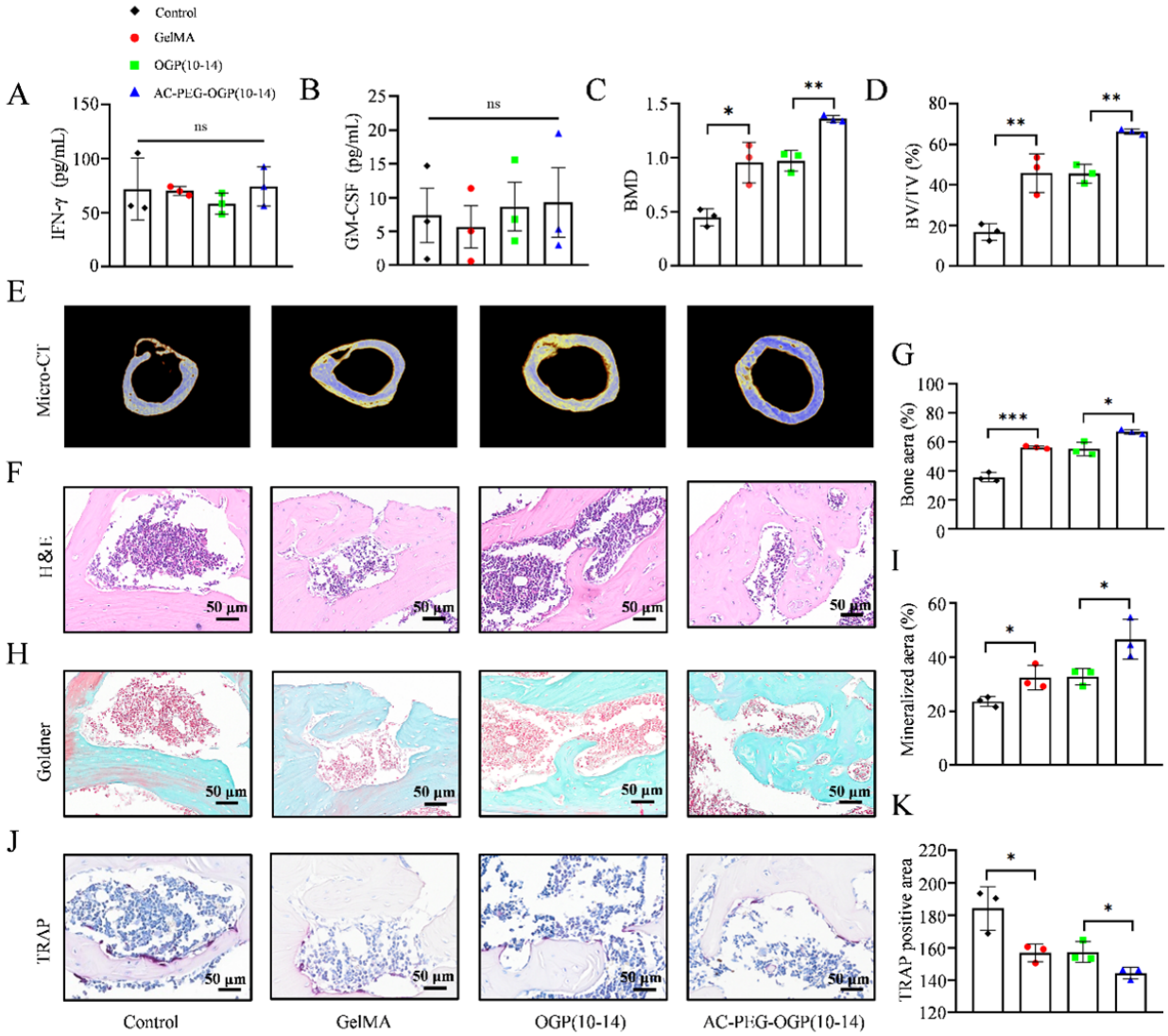

Fig. 6. Evaluation of the *in vivo* biocompatibility and bone repair performance of different hydrogels. (**A**) Serum levels of IFN-γ in mice. (**B**) Serum levels of GM-CSF in mice. (**C**,**D**) Quantitative evaluation of the micro-CT imaging parameters. (**E**) Micro-CT images. (**F**) HE staining images. (**G**) Statistical analysis of HE stained images. (**H**) Goldner's trichrome stained images. (**I**) Statistical analysis of Goldner's trichrome stained images. (**J**) TRAP stained images. (**K**) TRAP staining area statistics of bone defect tissues. n = 3. ns, not significant; *$p < 0.05$; **$p < 0.01$; ***$p < 0.001$. The scale bar represents 50 μm.

ministered to euthanize the mice, after which the femurs were extracted. The workflow of the animal experiments is shown in **Supplementary Fig. 1**.

ELISA Experiment

The concentrations of GM-CSF and IFN-γ in the serum were assessed using the mouse GM-CSF ELISA Kit and the mouse IFN-γ ELISA kit through OD value measurements.

Micro-Computed Tomography (CT) Imaging Analysis

Mouse femur samples were analyzed using the micro-CT scanning technique (Skycan 1272, Bruker, Billerica, MA, USA). After the defective region was identified, the region of interest (ROI) was reconstructed using the associated CTAn (1.20, Bruker Corporation, Billerica, MA, USA) and CTVol (2.3, Bruker Corporation, Billerica, MA, USA) software, and bone volume/tissue volume (BV/TV) and bone mineral density (BMD) were calculated.

Histological and Immunostaining Analysis

After decalcification, embedding, and sectioning, the mouse femur samples were stained with hematoxylin and eosin (HE), Goldner's trichrome, and TRAP. The area of new bone tissue and the distribution area of osteoclasts were calculated using ImageJ software. Mouse femur sections were stained with β-catenin and Col1a1 antibodies, and the mean optical density in the bone defect area was calculated

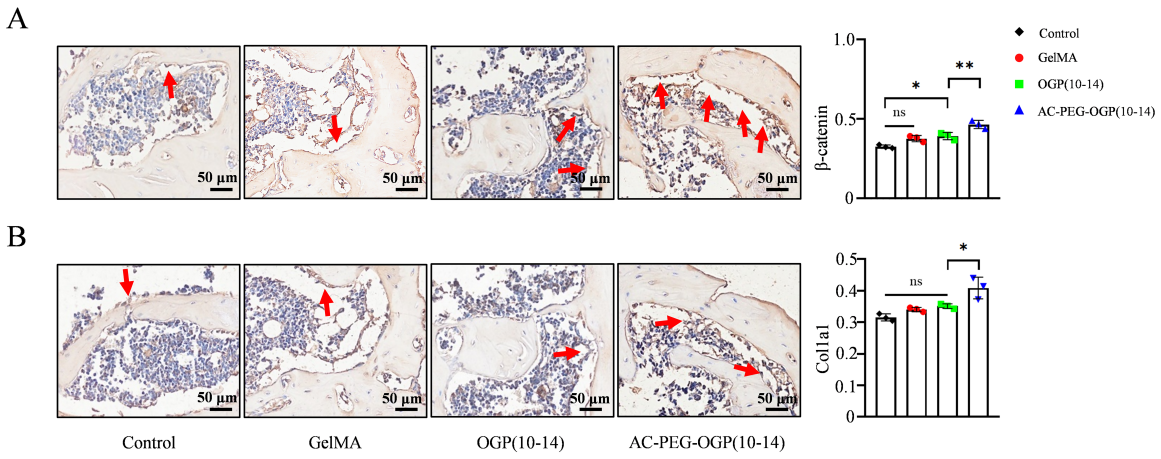

Fig. 7. Immunohistochemical analysis of bone defect tissues. (**A**) Immunohistochemical staining for *β-catenin* and statistical analysis. (**B**) Immunohistochemical staining for *Col1a1* and statistical analysis. The red arrow indicates the positive part. n = 3. ns, not significant; *$p < 0.05$; **$p < 0.01$. The scale bar represents 50 μm.

using ImageJ software. The antibodies used for immunohistochemistry are listed in **Supplementary Table 2**.

Data Analysis

All experiments were performed in three independent replicates to ensure reproducibility. Data were collected using Microsoft Excel (16.0, Microsoft Corporation, Redmond, WA, USA) and statistically analyzed using GraphPad Prism software (version 8.01, Graph-Pad Software, San Diego, CA, USA). Differences between two groups were analyzed using the Student's *t*-test. If the data from two groups are normally distributed and exhibit equal variance, a Student's *t*-test assuming homogeneity of variances is applied; otherwise, a *t*-test not assuming equal variances is used. If the data from both groups are not normally distributed, non-parametric tests are employed. Differences among multiple groups were analyzed using one-way ANOVA, followed by Tukey's post hoc test for multiple comparisons. Data are presented as the means ± standard deviations (SDs) or means ± standard error of the means. Significant differences are indicated as follows: *$p < 0.05$, **$p < 0.01$ and ***$p < 0.001$.

Results

Characterization of Materials

The reaction of AC-PEG-NHS with OGP(10-14) generates AC-PEG-OGP(10-14), as shown in Fig. 2**A**. These results showed that compared with AC-PEG-NHS, AC-PEG-OGP(10-14) has an additional amide bond. Therefore, in this study, the AC-PEG-OGP(10-14) and AC-PEG-NHS powders were examined by FTIR, which showed that new peaks at X = 1656 cm^{-1} and X = 1609 cm^{-1} for AC-PEG-OGP(10-14) compared with those for AC-PEG-NHS (Fig. 2**B**), indicating that OGP(10-14) was successfully linked to AC-PEG-NHS. The mold for synthesizing the composite material and an image of the AC-PEG-OGP(10-14) group are shown in **Supplementary Fig. 2A**. SEM revealed the microstructures of the three groups of composite materials, namely, GelMA, OGP(10-14) and AC-PEG-OGP(10-14). The results revealed that all three composite materials exhibited similar microstructures, with interconnected pores and no significant differences in pore size (Fig. 2**C,D**). Furthermore, no significant differences were observed in the porosity among the three materials (Fig. 2**E**). These results indicated that loading OGP(10-14) or AC-PEG-OGP(10-14) did not change the original microstructure of the GelMA scaffold.

The mechanical property and degradation rate of the GelMA, OGP(10-14), and AC-PEG-OGP(10-14) groups were measured to evaluate the changes in the composite materials. Rheological experiments revealed that, within the low-frequency range (10^{-1}–10 Hz), the storage modulus (G′) of all three hydrogel groups was higher than the loss modulus (G″), indicating a typical gel-like behavior (**Supplementary Fig. 3A**). Mechanical performance tests further demonstrated a consistent trend between Young's modulus (Fig. 2**F**) and compressive strength (**Supplementary Fig. 3B**). Notably, the AC-PEG-OGP(10-14) group exhibited significantly better mechanical properties compared to the OGP(10-14) group, while no significant differences were observed between the OGP(10-14) and GelMA groups. Degradation experiments (Fig. 2**G**) showed that the cumulative degradation of the AC-PEG-OGP(10-14) group was significantly reduced, indicating enhanced *in vitro* stability. *In vitro* release experiments

demonstrated that the cumulative release of the OGP(10-14) group reached 92.3 % within the first four days, whereas the cumulative release of the AC-PEG-OGP(10-14) group was significantly lower than that of the OGP(10-14) group, which was 60.5 % (Fig. 2**H**). These results indicate that the AC-PEG-OGP(10-14) group of composites can effectively slow the release of OGP(10-14). Cells extracted from neonatal mouse calvaria were subsequently cultured for 3 days. These cells were also free of mycoplasma contamination (**Supplementary Table 3**) and exhibited a short spindle or cuboidal shape, with overlapping growth and high cell density **(Supplementary Fig. 4A**). Flow cytometry analysis revealed that the mean fluorescence intensity of CD90 in these cells was significantly greater than that in the control group (**Supplementary Fig. 4C,D**). These results confirm that the cells are osteoblasts. Primary osteoblasts were seeded onto different materials, generating three cell-laden biomaterial groups: the GelMA group, the OGP(10-14) group, and the AC-PEG-OGP(10-14) group. Images of the AC-PEG-OGP(10-14) group of biomaterials are shown in **Supplementary Fig. 2B**. Twenty-four hours after the cells were planted onto the composites, 4′,6-diamidino-2-phenylindole (DAPI) staining experiments showed that cells were attached to the material (**Supplementary Fig. 5**). Further observation of the biomaterials with cells implanted for 3 days by SEM revealed cell distribution on the scaffold (Fig. 2**I**). These findings verify the successful fabrication of the sustained release hydrogels, which effectively support osteoblast incorporation.

Biocompatibility of the Sustained-Release Hydrogels

Biocompatibility assessment serves as a fundamental methodology for evaluating the biosafety of engineered biomaterials. A live/dead staining assay demonstrated robust cell viability across all experimental groups (Fig. 3**A,B**). WST-1 proliferation assays further substantiated these findings, showing that osteoblasts were able to achieve stable proliferation in all three biomaterials, and no significant difference was observed in proliferative activity among the groups (Fig. 3**C**). Taken together, the results showed that these biomaterials exhibited excellent biocompatibility with osteoblasts.

Sustained-Release Hydrogels Promote Osteogenic Differentiation In Vitro

In this study, the osteogenic potential of the biomaterials was thoroughly evaluated. The differentiation ability of osteoblasts was examined in three biomaterial groups: GelMA, OGP(10-14), and AC-PEG-OGP(10-14). The RT-qPCR results showed (Fig. 4**A**) that the expression of the osteogenic marker genes *Sp7*, *β-catenin*, and *c-myc* in the AC-PEG-OGP(10-14) group was significantly greater than that in the GelMA and OGP(10-14) groups. ALP staining of osteoblasts embedded in the scaffolds demonstrated markedly enhanced enzymatic activity in the AC-PEG-OGP(10-14) group compared with that in the other groups (Fig. 4**B**). Furthermore, after the above three groups of biomaterials were incubated for 14 days, their osteogenic mineralization capacity was examined by ARS staining, and the formation of orange-red chelate complexes was used as an indicator of mineralization. Quantitative mineralization assays revealed significantly enhanced mineralization rates in the AC-PEG-OGP(10-14) group than in both the GelMA and OGP(10-14) control groups (Fig. 4**C**). These findings indicate that the AC-PEG-OGP(10-14) sustained-release hydrogel possesses superior osteogenic potential.

In the process of bone repair, the role of materials in osteoblasts in the bone microenvironment is crucial. Therefore, in this study, the extract solution of the biomaterial was further co-cultured with osteoblasts to verify its effects on the differentiation of primary osteoblasts in the bone microenvironment. Osteoblasts were cultured with the three groups of extract solutions for 7 days, RT-qPCR results revealed that the expression of the osteogenic marker genes *Col1a1*, *β-catenin*, and *c-myc* was significantly greater in the AC-PEG-OGP(10-14) group than in the GelMA and OGP(10-14) groups (Fig. 4**D**). Moreover, ALP staining revealed that compared with the GelMA and OGP(10-14) groups, the AC-PEG-OGP(10-14) group had significantly increased ALP expression (Fig. 4**E**). After co-culture for 14 days, the ARS staining results further confirmed that the mineralization capacity of osteoblasts in the bone-promoting microenvironment of the AC-PEG-OGP(10-14) group was significantly stronger than that of the GelMA and OGP(10-14) groups (Fig. 4**F**). These results indicated that compared with the GelMA and OGP(10-14) groups, the AC-PEG-OGP(10-14) group had a significant advantage in promoting osteogenic differentiation in the bone microenvironment.

Sustained-Release Hydrogels Inhibit BMM Differentiation In Vitro

To evaluate the effects of the materials on osteoclasts, conditioned media were prepared using extracts of the biomaterials and co-cultured with BMMs in cell culture plates. First, cells extracted from mouse bone marrow were cultured for 3 days. These cells were free of mycoplasma contamination (**Supplementary Table 3**), exhibited a round or oval shape with a regular morphology (**Supplementary Fig. 4B**), and had a significantly greater mean fluorescence intensity of F4/80 than the control group according to flow cytometry analysis (**Supplementary Fig. 4E,F**), confirming their identity as BMMs. BMMs were subsequently cultured in conditioned media for an additional 4 days. The effects of these biomaterials on the differentiation of BMMs were assessed using RT-qPCR and TRAP staining. Compared with those in the GelMA group, the expression levels of the osteoclast differentiation marker genes *MMP9* and *CTSK* in the OGP(10-14) and AC-PEG-OGP(10-14) groups were significantly lower (Fig. 5**A,B**). TRAP stain-

ing revealed that the TRAP-stained areas in the OGP(10-14) and AC-PEG-OGP(10-14) groups were significantly decreased (Fig. 5**C,D**). These experimental results indicate that the GelMA hydrogel scaffold containing OGP(10-14) can effectively inhibit the differentiation of BMMs.

Sustained-Release Hydrogels Promote Bone Defect Repair In Vivo

To evaluate the bone repair ability of biomaterials *in vivo*, this study involved construction of a femoral defect model in C57BL/6 mice and biomaterials were implanted in the region of bone defects. The immune response is an important indicator for assessing the biocompatibility of biomaterials *in vivo*. Therefore, serum samples were collected 4 weeks post-implantation to analyze immune rejection. The results revealed no significant differences in the levels of the immune factors GM-CSF and IFN-γ among the control, GelMA, OGP(10-14), and AC-PEG-OGP(10-14) groups (Fig. 6**A,B**). These results indicate that the AC-PEG-OGP(10-14) group exhibited excellent biocompatibility *in vivo*.

Micro-CT scanning was used to evaluate the bone histomorphometry of femoral defects repaired for 4 weeks. Quantitative analysis methods were applied to assess the BMD and BV/TV in the defect areas across the four experimental groups. The results revealed that the BMD values in the AC-PEG-OGP(10-14) group were significantly greater than those in the control, GelMA, and OGP(10-14) groups. Similarly, the BV/TV values in the AC-PEG-OGP(10-14) group were significantly greater than those in the other three groups (Fig. 6**C,D**). Three-dimensional reconstruction revealed that the AC-PEG-OGP(10-14) group had the greatest amount of new bone formation, which almost completely repaired the bone defect area. The new bone generation in the OGP(10-14) group was less than that in the AC-PEG-OGP(10-14) group, with small gaps still evident in the defect area. The bone defect areas in the GelMA group and the control group remained relatively obvious (Fig. 6**E**).

Further histochemical analysis of the repaired bone tissue was conducted. The results of HE staining and Goldner's trichrome staining were consistent with the results of the micro-CT scan. Compared with the control group, the GelMA, OGP(10-14), and AC-PEG-OGP(10-14) groups all showed significant increase in new bone volume. As shown in Fig. 6**F–I** (**Supplementary Fig. 6** for scale-down multiples), the amount of new bone was significantly greater in the AC-PEG-OGP(10-14) group than in the other groups. Furthermore, TRAP staining revealed that the number of TRAP-positive cells in the AC-PEG-OGP(10-14) group was significantly lower than that in the other three groups, indicating significant inhibition of osteoclast formation (Fig. 6**J,K**). These findings collectively demonstrate that the AC-PEG-OGP(10-14) sustained-release hydrogel has high potential for promoting bone defect repair.

Sustained-Release Hydrogels May Promote Bone Defect Repair via the Wnt/β-Catenin Signaling Pathway

Immunohistochemical analysis of bone defect tissues was performed in this study. The results of the analysis revealed that the protein expression of *β-catenin* in osteoblasts was significantly greater in the AC-PEG-OGP(10-14) group than in the OGP(10-14) group, the GelMA group, and the control group, with the lowest expression in the control group (Fig. 7**A**). Further analysis of the osteogenic marker *Col1a1* revealed significantly higher protein expression in the AC-PEG-OGP(10-14) group than in the other groups (Fig. 7**B**). Notably, *Col1a1* serves not only as a crucial osteogenic marker but also as a key effector in the Wnt/*β-catenin* signaling pathway. Collectively, these results demonstrate that the AC-PEG-OGP(10-14) group enhances bone defect repair through the activation of the Wnt/*β-catenin* signaling pathway, which is accompanied by the upregulation of both *β-catenin* and *Col1a1* expression.

Discussion

In tissue engineering, bioscaffold materials, seed cells, and growth factors together constitute the three core elements of bone tissue engineering. In this study, a novel composite material with a sustained OGP(10-14) release capability was developed through the incorporation of AC-PEG-NHS as a crosslinking molecule. FTIR experiment showed that new peaks at X = 1656 cm^{-1} and X = 1609 cm^{-1} for AC-PEG-OGP(10-14) compared with those for AC-PEG-NHS. According to previous studies [33,34], X = 1656 cm^{-1} is an amide I group (C = O), and X = 1609 cm^{-1} is an amide II group (N-H), indicating that OGP(10-14) was successfully linked to AC-PEG-NHS. From a structural standpoint, the composite material retains the inherent porous structure of GelMA while maintaining good connectivity between these pores. This unique structural design provides an ideal attachment environment for cells, greatly facilitating the exchange of substances between cells and the external environment, which has an extremely important positive effect on cell growth and differentiation [35–37]. Bone tissue repair is a long-term biological process, during which materials implanted into the bone defect are required to withstand sustained mechanical stress in the physiological environment. Therefore, the mechanical properties and the degradation rate of scaffold materials are significant indicators for evaluating bone repair scaffold materials [38–40]. The current study had improved the mechanical strength of GelMA and decreased the rate of decline by adjusting the crosslinking reaction with GelMA [41,42]. This experiment enhanced the structural stability of the material by crosslinking the double bonds in GelMA with AC-PEG-NHS, thereby improving its mechanical properties and reducing the degradation rate.

In bone repair materials, functional molecules can rapidly diffuse through the pores of the material, reduc-

ing the effectiveness of functional molecules. Studies have been conducted to establish a physical barrier to slow the rate of growth factor release using microsphere encapsulation. For example, Ma *et al*. [43] encapsulated OGP peptides and constructed AL-PLGA@PNPs nanoparticles to achieve slow release of OGP. However, their results showed that the cumulative release rate of the peptide was already close to 80 % by Day 4. In contrast, the present study used a different strategy: OGP(10-14) polypeptide was modified with AC-PEG-NHS to form AC-PEG-OGP(10-14), and then AC-PEG-OGP(10-14) was attached to the GelMA scaffold. The experimental results of this method showed that only 60.50 % of the OGP(10-14) polypeptide was released during the first 4 days, and the release rate stabilized after the 4th day. In addition, the release rate of the peptide from the composite material was consistent with its degradation rate, leading us to speculate that the peptide is released as the composite material degrades. This sustained release mode provides a more stable osteogenic microenvironment for the bone defect area, which is conducive to the promotion of cell differentiation and new bone formation, further ensuring the continuity and effectiveness of the repair and regeneration process. This is crucial for improving the efficacy of bone repair materials.

Biocompatibility experiments demonstrated that the biomaterial exhibited good biocompatibility, supporting osteoblast survival and maintaining a stable proliferative state within the material. An important objective of biomaterials is that the materials themselves can undergo osteogenic differentiation and mineralization [44]. The sustained release of OGP(10-14) from the sustained-release GelMA scaffold material provides a stable microenvironment for osteoblasts. *In vitro* studies revealed that the sustained-release GelMA scaffold material not only significantly enhanced the differentiation and mineralization of encapsulated osteoblasts but also promoted these effects in co-cultured osteoblasts. Bone homeostasis is a dynamic balance process between bone resorption and bone formation, which is accomplished mainly by the synergistic action of osteoclasts and osteoblasts. Study has shown that overactivation of osteoclasts can affect bone regeneration [45]. Liu *et al*. [46] reported that OGP promoted the differentiation and mineralization of osteoblasts and the secretion of OPG, which combined with RANKL, thus obstructing the binding of RANK and RANKL, inhibiting the activation of the RANKL-RANK signaling pathway, and inhibiting the differentiation and activity of osteoclasts. These findings are consistent with our findings that biomaterials containing OGP(10-14) significantly inhibit BMM differentiation into osteoclasts. In terms of new bone formation ability, the AC-PEG-OGP(10-14) sustained-release GelMA scaffold showed excellent bone defect repair ability and significantly outperformed the OGP(10-14) group, GelMA group and the control group. These findings suggest that biomaterials carrying seeded primary osteoblasts and possessing sustained-release OGP(10-14) exhibit stronger bone defect repair ability. High-viability implantation of osteoblasts and controlled slow release of OGP(10-14) at the bone defect site through bone tissue engineering technology may be effective strategies for overcoming current bone defect repair problems.

β-catenin is a crucial regulatory factor in the Wnt/*β-catenin* signaling pathway, and its activation promotes the proliferation and differentiation of osteoblasts [47,48]. Additionally, *Col1a1* is both an osteogenic differentiation effector in the Wnt/*β-catenin* signaling pathway and a major component of newly formed bone [46,49,50]. A series of experiments conducted by Shou *et al*. [51] confirmed that biomaterials loaded with OGP could significantly enhance the gene expression of *β-catenin*, *OCN*, *OPN* and *Col1a1* in MC3T3-E1 pre-osteoblasts. After small interfering RNA (siRNA)-mediated knockdown of *β-catenin*, the expression levels of these osteogenic markers were significantly downregulated. In this study, immunohistochemical analysis revealed that AC-PEG-OGP(10-14) group could significantly enhance the protein expression of *β-catenin* and *Col1a1*, and RT-qPCR test results also confirmed that the material could increase the gene expression of *β-catenin* and *Col1a1*. These data collectively support that the sustained-release hydrogel scaffold AC-PEG-OGP(10-14) likely exerts its effects through activation of the Wnt/*β-catenin* signaling pathway.

Although slow-release hydrogel materials demonstrate considerable potential in promoting bone regeneration, this study has certain limitations. First, regarding the evaluation of degradation properties, only *in vitro* degradation experiments were conducted. The degradation behavior *in vivo* remains unexamined, and it is unclear whether its degradation kinetics phase matches with the bone regeneration process. Second, while RT-qPCR and immunohistochemistry results indirectly suggest that the material may facilitate bone defect repair by modulating the Wnt/*β-catenin* signaling pathway, the specific mechanisms underlying this pathway have not been thoroughly elucidated. Further studies employing Western blot analysis, such as examining total *β-catenin* levels and expression changes of downstream target molecules, could provide more direct evidence to clarify the mechanistic involvement of this pathway. Third, the number of animal samples in each group in the *in vivo* experiments was small (n = 3). Although the results showed a certain trend, this small sample size limited the statistical power and the generalizability of the conclusions. Therefore, in the future study, further validation is needed through animal experiments with larger sample sizes to ensure the robustness and reproducibility of the results.

Conclusions

In this study, a novel slow-release hydrogel was successfully constructed based on tissue engineering princi-

ples, and its effect on bone defect repair was evaluated. The experimental results showed that the composite not only maintained the porous structure and biocompatibility of the GelMA scaffold but also significantly improved the mechanical properties of the material, effectively slowing the degradation rate of the material through the introduction of AC-PEG-NHS and achieving the sustained release of OGP(10-14). *In vitro* experiments indicated that the composite material promoted osteogenic differentiation and mineralization and inhibited BMM differentiation. *In vivo* experiments revealed that four weeks after implantation, the composite material significantly improved the efficiency of bone defect repair, accelerated the process of defect repair and increased the amount of new bone. Mechanistic studies revealed that sustained-release hydrogel could promote bone defect repair by activating Wnt/β-*catenin* signaling in osteoblasts. Preliminary research indicated that the sustained-release hydrogel is a biomaterial with good biocompatibility, mechanical properties, and the ability to slowly release OGP(10-14), which has great potential for application in the field of bone defect repair.

List of Abbreviations

ALP, alkaline phosphatase; ARS, Alizarin Red S; BMMs, bone marrow-derived macrophages; BV/TV, bone volume/tissue volume; BMD, bone mineral density; ECM, extracellular matrix; FTIR, fourier transform infrared spectroscopy; GelMA, gelatin methacryloyl; HE, hematoxylin and eosin; OGP, osteogenic growth peptide; OD, optical density; SEM, scanning electron microscopy; TRAP, tartrate-resistant acid phosphatase; AC-PEG-NHS, acryloylated polyethylene glycol N-hydroxysuccinimide; BCA, bicinchoninic acid; BMP, bone morphogenetic protein; M-CSF, macrophage colony-stimulating factor; IFN-γ, interferon-γ; PBS, phosphate buffered saline; mRNA, messenger RNA; RT-qPCR, reverse transcription quantitative polymerase chain reaction; RANKL, receptor activator of nuclear factor-κB ligand; CT, computed tomography; GM-CSF, granulocyte-macrophage colony-stimulating factor.

Availability of Data and Materials

All datasets generated or analyzed during the current study are included in this published article and its Supplementary Information. Additional experimental details and more detailed data used or analyzed in this study are available from the corresponding author upon reasonable request.

Author Contributions

LYL, FCZ, SWD and JML contributed to the design of this work. LYL, FCZ and YWH contributed to the interpretation of data. LYL, FCZ, and YWH analyzed the data. LYL and FCZ drafted the work. JML and SWD revised critically for important intellectual content. All authors read and approved the final manuscript. All authors agreed to be accountable for all aspects of the work in ensuring that questions related to the accuracy or integrity of any part of the work were appropriately investigated and resolved.

Ethics Approval and Consent to Participate

All animal procedures were performed in accordance with the Guidelines for the Care and Use of Laboratory Animals of the Third Military Medical University. The study was approved by the Institutional Animal Care and Use Committee of the Third Military Medical University (AMUWEC20230200).

Acknowledgments

Not applicable.

Funding

This work was financially supported by the Integration Project of NSFC Joint Fund for Regional Innovation and Development (U23A6008), the General Program of National Natural Science Foundation of China (82572838), the Youth Program of National Natural Science Foundation of China (82002316), and the General Program of Natural Science Foundation of Chongqing (CSTB2023NSCQ-MSX0026).

Conflict of Interest

The author(s) declared no potential conflicts of interest with respect to the research, authorship, and/or publication of this article.

Supplementary Material

Supplementary material associated with this article can be found, in the online version, at https://doi.org/10.22203/eCM.v055a02.

References

[1] Gao X, Ruzbarsky JJ, Layne JE, Xiao X, Huard J. Stem Cells and Bone Tissue Engineering. Life. 2024; 14: 287. https://doi.org/10.3390/life14030287.

[2] Zhang J, Hu W, Zou Z, Li Y, Kang F, Li J, *et al*. The role of lipid metabolism in osteoporosis: Clinical implication and cellular mechanism. Genes & Diseases. 2023; 11: 101122. https://doi.org/10.1016/j.gendis.2023.101122.

[3] Migliorini F, La Padula G, Torsiello E, Spiezia F, Oliva F, Maffulli N. Strategies for large bone defect reconstruction after trauma, infections or tumour excision: a comprehensive review of the literature. European Journal of Medical Research. 2021; 26: 118. https://doi.org/10.1186/s40001-021-00593-9.

[4] Kinaia BM, Daweri O, Gala R, Turows A, Harunani A, Neely AL. Management of vertical bony defect using novel xenogeneic/allogeneic bone graft: A case report. Clinical Advances in Periodontics. 2024; 14: 95–99. https://doi.org/10.1002/cap.10256.

[5] Shi Z, Zhong Q, Chen Y, Gao J, Pan X, Lian Q, *et al*. Nanohydroxyapatite, Nanosilicate-Reinforced Injectable, and Biomimetic Gelatin-Methacryloyl Hydrogel for Bone Tissue Engineering. In-

ternational Journal of Nanomedicine. 2021; 16: 5603–5619. https://doi.org/10.2147/IJN.S321387.

[6] Gillman CE, Jayasuriya AC. FDA-approved bone grafts and bone graft substitute devices in bone regeneration. Materials Science & Engineering. C, Materials for Biological Applications. 2021; 130: 112466. https://doi.org/10.1016/j.msec.2021.112466.

[7] Yuan X, Zhu W, Yang Z, He N, Chen F, Han X, *et al*. Recent Advances in 3D Printing of Smart Scaffolds for Bone Tissue Engineering and Regeneration. Advanced Materials. 2024; 36: e2403641. https://doi.org/10.1002/adma.202403641.

[8] Jiang F, Qi X, Wu X, Lin S, Shi J, Zhang W, *et al*. Regulating macrophage-MSC interaction to optimize BMP-2-induced osteogenesis in the local microenvironment. Bioactive Materials. 2023; 25: 307–318. https://doi.org/10.1016/j.bioactmat.2023.02.001.

[9] Luther G, Wagner ER, Zhu G, Kang Q, Luo Q, Lamplot J, *et al*. BMP-9 induced osteogenic differentiation of mesenchymal stem cells: molecular mechanism and therapeutic potential. Current Gene Therapy. 2011; 11: 229–240. https://doi.org/10.2174/156652311795684777.

[10] Rochira A, Siculella L, Damiano F, Palermo A, Ferrante F, Carluccio MA, *et al*. Concentrated Growth Factors (CGF) Induce Osteogenic Differentiation in Human Bone Marrow Stem Cells. Biology. 2020; 9: 370. https://doi.org/10.3390/biology9110370.

[11] Lee S, Kim JH, Kim YH, Hong J, Kim WK, Jin S, *et al*. Sustained BMP-2 delivery via alginate microbeads and polydopamine-coated 3D-Printed PCL/β-TCP scaffold enhances bone regeneration in long bone segmental defects. Journal of Orthopaedic Translation. 2024; 49: 11–22. https://doi.org/10.1016/j.jot.2024.08.013.

[12] Zhang L, Ji C, Li Z, Jiwa H, Xie Z, Luo X, *et al*. Sonic Hedgehog potentiates BMP9-induced osteogenic differentiation of mesenchymal stem cells. Genes & Diseases. 2024; 12: 101308. https://doi.org/10.1016/j.gendis.2024.101308.

[13] Li H, Zhang X, Ameer KA, Zhang X, Du W, Mei S, *et al*. Clinical observation of concentrated growth factor (CGF) combined with iliac cancellous bone and composite bone material graft on postoperative osteogenesis and inflammation in the repair of extensive mandibular defects. Journal of Stomatology, Oral and Maxillofacial Surgery. 2023; 124: 101472. https://doi.org/10.1016/j.jormas.2023.101472.

[14] Purbantoro SD, Osathanon T, Nantavisai S, Sawangmake C. Osteogenic growth peptide enhances osteogenic differentiation of human periodontal ligament stem cells. Heliyon. 2022; 8: e09936. https://doi.org/10.1016/j.heliyon.2022.e09936.

[15] Zuo Y, Xiong Q, Li Q, Zhao B, Xue F, Shen L, *et al*. Osteogenic growth peptide (OGP)-loaded amphiphilic peptide (NapFFY) supramolecular hydrogel promotes osteogenesis and bone tissue reconstruction. International Journal of Biological Macromolecules. 2022; 195: 558–564. https://doi.org/10.1016/j.ijbiomac.2021.12.028.

[16] Zhong J, Huang J, Chen L, Duan J. Construction of a biocompatible MWCNTs-chitosan composite interface and its application to impedance cytosensing of osteoblastic MC3T3-E1 cells. RSC Advances. 2022; 12: 31663–31670. https://doi.org/10.1039/d2ra05995a.

[17] Raphael-Mizrahi B, Attar-Namdar M, Chourasia M, Cascio MG, Shurki A, Tam J, *et al*. Osteogenic growth peptide is a potent anti-inflammatory and bone preserving hormone via cannabinoid receptor type 2. eLife. 2022; 11: e65834. https://doi.org/10.7554/eLife.65834.

[18] Pigossi SC, Medeiros MC, Saska S, Cirelli JA, Scarel-Caminaga RM. Role of Osteogenic Growth Peptide (OGP) and OGP(10-14) in Bone Regeneration: A Review. International Journal of Molecular Sciences. 2016; 17: 1885. https://doi.org/10.3390/ijms17111885.

[19] Chen YC, Bab I, Mansur N, Muhlrad A, Shteyer A, Namdar-Attar M, *et al*. Structure-bioactivity of C-terminal pentapeptide of osteogenic growth peptide [OGP(10-14)]. The Journal of Peptide Research: Official Journal of the American Peptide Society. 2000; 56: 147–156. https://doi.org/10.1034/j.1399-3011.2000.00763.x.

[20] Shu F, Huang H, Xiao S, Xia Z, Zheng Y. Netrin-1 co-cross-linked hydrogel accelerates diabetic wound healing *in situ* by modulating macrophage heterogeneity and promoting angiogenesis. Bioactive Materials. 2024; 39: 302–316. https://doi.org/10.1016/j.bioactmat.2024.04.019.

[21] Jiang X, Li D, Tassey J, Li J, Liu J, Li G, *et al*. Complex hydrogel for cartilage regeneration and anti-inflammation. Composites Part B: Engineering. 2024; 280: 111481. https://doi.org/10.1016/j.compositesb.2024.111481.

[22] Zhou B, Jiang X, Zhou X, Tan W, Luo H, Lei S, *et al*. GelMA-based bioactive hydrogel scaffolds with multiple bone defect repair functions: therapeutic strategies and recent advances. Biomaterials Research. 2023; 27: 86. https://doi.org/10.1186/s40824-023-00422-6.

[23] Mamidi N, Ijadi F, Norahan MH. Leveraging the Recent Advancements in GelMA Scaffolds for Bone Tissue Engineering: An Assessment of Challenges and Opportunities. Biomacromolecules. 2024; 25: 2075–2113. https://doi.org/10.1021/acs.biomac.3c00279.

[24] Pramanik S, Alhomrani M, Alamri AS, Alsanie WF, Nainwal P, Kimothi V, *et al*. Unveiling the versatility of gelatin methacryloyl hydrogels: a comprehensive journey into biomedical applications. Biomedical Materials. 2024; 19. https://doi.org/10.1088/1748-605X/ad4df7.

[25] Arambula-Maldonado R, Mequanint K. Osteogenic Differentiation Potential of iMSCs on GelMA-BG-MWCNT Nanocomposite Hydrogels. Biomimetics. 2024; 9: 338. https://doi.org/10.3390/biomimetics9060338.

[26] Ganguly K, Dutta SD, Randhawa A, Patel DK, Patil TV, Lim KT. Transcriptomic Changes toward Osteogenic Differentiation of Mesenchymal Stem Cells on 3D-Printed GelMA/CNC Hydrogel under Pulsatile Pressure Environment. Advanced Healthcare Materials. 2023; 12: e2202163. https://doi.org/10.1002/adhm.202202163.

[27] Ai Y, Dai F, Li W, Xu F, Yang H, Wu J, *et al*. Photo-crosslinked bioactive BG/BMSCs@GelMA hydrogels for bone-defect repairs. Materials Today. Bio. 2023; 23: 100882. https://doi.org/10.1016/j.mtbio.2023.100882.

[28] Zhu M, Zhang H, Zhou Q, Sheng S, Gao Q, Geng Z, *et al*. Dynamic GelMA/DNA Dual-Network Hydrogels Promote Woven Bone Organoid Formation and Enhance Bone Regeneration. Advanced Materials. 2025; 37: e2501254. https://doi.org/10.1002/adma.202501254.

[29] Huan Y, Zhou D, Wu X, He X, Chen H, Li S, *et al*. 3D bioprinted autologous bone particle scaffolds for cranioplasty promote bone regeneration with both implanted and native BMSCs. Biofabrication. 2023; 15. https://doi.org/10.1088/1758-5090/acbe21.

[30] Luo P, Cheng Y, Luo Y, Zhang N, Cao J, Wang H, *et al*. Hydrogel Enhanced Organoid Multidirectional Differentiation via Yap/Tead4 Mechanotransduction for Accelerated Tissue Regeneration. ACS Applied Materials & Interfaces. 2025; 17: 37601–37616. https://doi.org/10.1021/acsami.5c06161.

[31] Pezeshki-Modaress M, Zandi M, Rajabi S. Tailoring the gelatin/chitosan electrospun scaffold for application in skin tissue engineering: an *in vitro* study. Progress in Biomaterials. 2018; 7: 207–218. https://doi.org/10.1007/s40204-018-0094-1.

[32] Mesgar AS, Mohammadi Z, Khosrovan S. Improvement of mechanical properties and *in vitro* bioactivity of freeze-dried gelatin/chitosan scaffolds by functionalized carbon nanotubes. International Journal of Polymeric Materials and Polymeric Biomaterials. 2017; 67: 267–276. https://doi.org/10.1080/00914037.2017.1320663.

[33] Man VH, He X, Nguyen PH, Sagui C, Roland C, Xie XQ, *et al*. Unpolarized laser method for infrared spectrum calculation of amide I CO bonds in proteins using molecular dynamics simulation. Computers in Biology and Medicine. 2023; 159: 106902. https://doi.org/10.1016/j.compbiomed.2023.106902.

[34] Durak T, Ciak B, Durak R, Depciuch J. Application of ATR-Fourier transform infrared spectroscopy in fast and simultaneous determina-

tion of leaf chemical and functional properties of forest herb species. Talanta. 2025; 289: 127738. https://doi.org/10.1016/j.talanta.2025.127738.

[35] Shirzad M, Zolfagharian A, Matbouei A, Bodaghi M. Design, evaluation, and optimization of 3D printed truss scaffolds for bone tissue engineering. Journal of the Mechanical Behavior of Biomedical Materials. 2021; 120: 104594. https://doi.org/10.1016/j.jmbbm.2021.104594.

[36] Rezania N, Asadi-Eydivand M, Abolfathi N, Bonakdar S, Mehrjoo M, Solati-Hashjin M. Three-dimensional printing of polycaprolactone/hydroxyapatite bone tissue engineering scaffolds mechanical properties and biological behavior. Journal of Materials Science. Materials in Medicine. 2022; 33: 31. https://doi.org/10.1007/s10856-022-06653-8.

[37] Toosi S, Javid-Naderi MJ, Tamayol A, Ebrahimzadeh MH, Yaghoubian S, Mousavi Shaegh SA. Additively manufactured porous scaffolds by design for treatment of bone defects. Frontiers in Bioengineering and Biotechnology. 2024; 11: 1252636. https://doi.org/10.3389/fbioe.2023.1252636.

[38] Georgantzinos SK. Multiscale Simulation of Composite Structures: Damage Assessment, Mechanical Analysis and Prediction. Materials. 2022; 15: 6494. https://doi.org/10.3390/ma15186494.

[39] Stirnemann G. Recent Advances and Emerging Challenges in the Molecular Modeling of Mechanobiological Processes. The Journal of Physical Chemistry. B. 2022; 126: 1365–1374. https://doi.org/10.1021/acs.jpcb.1c10715.

[40] Tajvar S, Hadjizadeh A, Samandari SS. Scaffold degradation in bone tissue engineering: An overview. International Biodeterioration & Biodegradation. 2023; 180: 105599. https://doi.org/10.1016/j.ibiod.2023.105599.

[41] Hafezi M, Khorasani SN, Khalili S, Neisiany RE. Self-healing interpenetrating network hydrogel based on GelMA/alginate/nanoclay. International Journal of Biological Macromolecules. 2023; 242: 124962. https://doi.org/10.1016/j.ijbiomac.2023.124962.

[42] Wang Y, Cao X, Ma M, Lu W, Zhang B, Guo Y. A GelMA-PEGDA-nHA Composite Hydrogel for Bone Tissue Engineering. Materials. 2020; 13: 3735. https://doi.org/10.3390/ma13173735.

[43] Ma S, Xu S, Li M, Du Y, Tian G, Deng J, *et al*. A Bone Targeting Nanoparticle Loaded OGP to Restore Bone Homeostasis for Osteoporosis Therapy. Advanced Healthcare Materials. 2023; 12: e2300560. https://doi.org/10.1002/adhm.202300560.

[44] Wang J, Wu Y, Li G, Zhou F, Wu X, Wang M, *et al*. Engineering Large-Scale Self-Mineralizing Bone Organoids with Bone Matrix-Inspired Hydroxyapatite Hybrid Bioinks. Advanced Materials. 2024; 36: e2309875. https://doi.org/10.1002/adma.202309875.

[45] Veis DJ, O'Brien CA. Osteoclasts, Master Sculptors of Bone. Annual Review of Pathology. 2023. 18: 257–281. https://doi.org/10.1146/annurev-pathmechdis-031521-040919.

[46] Liu J, Tang Y, Yang W, Tao B, He Y, Shen X, *et al*. Functionalization of titanium substrate with multifunctional peptide OGP-NAC for the regulation of osteoimmunology. Biomaterials Science. 2019; 7: 1463–1476. https://doi.org/10.1039/c8bm01611a.

[47] Wang X, Qu Z, Zhao S, Luo L, Yan L. Wnt/β-catenin signaling pathway: proteins' roles in osteoporosis and cancer diseases and the regulatory effects of natural compounds on osteoporosis. Molecular Medicine. 2024; 30: 193. https://doi.org/10.1186/s10020-024-00957-x.

[48] Hu L, Chen W, Qian A, Li YP. Wnt/β-catenin signaling components and mechanisms in bone formation, homeostasis, and disease. Bone Research. 2024; 12: 39. https://doi.org/10.1038/s41413-024-00342-8.

[49] Han R, Zhang W, Zhang L, Zou J, Yang Y, Li H, *et al*. Notoginsenoside R1 Promotes Proliferation and Osteogenic Differentiation of hPDLSCs via Wnt/β-Catenin Signaling Pathway. Drug Design, Development and Therapy. 2022; 16: 4399–4409. https://doi.org/10.2147/DDDT.S387004.

[50] Qi HZ, Ye YL, Suo Y, Qu H, Zhang HY, Yang KB, *et al*. Wnt/β-catenin signaling mediates the abnormal osteogenic and adipogenic capabilities of bone marrow mesenchymal stem cells from chronic graft-versus-host disease patients. Cell Death & Disease. 2021; 12: 308. https://doi.org/10.1038/s41419-021-03570-6.

[51] Shou Z, Bai Z, Zhou H, Shen Y, Huang X, Meng H, *et al*. Engineering tunable dual peptide hybrid coatings promote osseointegration of implants. Materials Today. Bio. 2023; 24: 100921. https://doi.org/10.1016/j.mtbio.2023.100921.

Editor's note: The Scientific Editor responsible for this paper was Fergal J. O'Brien.

Received: 15th April 2025; **Accepted**: 9th December 2025; **Published**: 30th January 2026